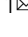


## Electrical characterisation of higher order spin wave modes in vortex-based magnetic tunnel junctions

Alex. S. Jenkins <sup>1</sup>, Lara San Emeterio Alvarez<sup>1</sup>, Samh Memshawy<sup>2</sup>, Paolo Bortolotti<sup>2</sup>, Vincent Cros <sup>2</sup>, Paulo P. Freitas<sup>1</sup> & Ricardo Ferreira<sup>1</sup>

NiFe-based vortex spin-torque nano-oscillators (STNO) have been shown to be rich dynamic systems which can operate as efficient frequency generators and detectors, but with a limitation in frequency determined by the gyrotropic frequency, typically sub-GHz. In this report, we present a detailed analysis of the nature of the higher order spin wave modes which exist in the Super High Frequency range (3–30 GHz). This is achieved via micro-magnetic simulations and electrical characterisation in magnetic tunnel junctions, both directly via the spin-diode effect and indirectly via the measurement of the coupling with the gyrotropic critical current. The excitation mechanism and spatial profile of the modes are shown to have a complex dependence on the vortex core position. Additionally, the inter-mode coupling between the fundamental gyrotropic mode and the higher order modes is shown to reduce or enhance the effective damping depending upon the sense of propagation of the confined spin wave.

<sup>1</sup>International Iberian Nanotechnology Laboratory, Braga, Portugal. <sup>2</sup>Unité Mixte de Physique, CNRS, Thales, Université Paris-Saclay, Palaiseau, France.  
email: [alex.jenkins@inl.int](mailto:alex.jenkins@inl.int)

Spintronics, which is based on the detection and manipulation of the spin of an electron, is a wide-ranging field of research with many novel nanotechnology solutions for the increasing challenges encountered by conventional electronic systems related to miniaturization, power consumption and device robustness. Two of the main pillars representing emerging dynamic spintronics technologies are spin-torque nano-oscillators (STNOs)<sup>1–9</sup> and spin-wave-based spintronics or magnonics<sup>10</sup>. STNOs typically harness the spin-polarized current-induced dynamical behaviour in a ferromagnet/spacer/ferromagnet trilayer configuration, where the spacer can be either metallic (i.e., spin valve<sup>1,2</sup>) or an insulator (i.e., magnetic tunnel junction (MTJ))<sup>4,5</sup>, and which can either be fully confined in nanopillars<sup>1,2,4,5</sup> or have a nanocontact geometry<sup>11</sup>. Magnonics is the engineering of the dispersion relation and the control of propagation of spin waves in ferromagnetic nanostructures<sup>12</sup>, and has been proposed for a range of Information and communications technology (ICT) applications including beyond-CMOS (Complementary Metal Oxide Semiconductor) computing and high-frequency signal processing<sup>10,13</sup>.

There has been some recent study focussed on the overlap between STNOs and magnonics, and these include relatively diverse experiments ranging from the spin wave-mediated synchronization of nanocontact oscillators<sup>14,15</sup> to the emission of spin waves by magnetic vortices during vortex core displacement<sup>16,17</sup> and reversal<sup>18,19</sup>, and the exploration of higher-order spin-wave modes<sup>20–27</sup> associated with magnetic vortices, the latter of these being the focus of this study.

Several spin-wave modes have been previously associated with magnetic vortices, having been found to exist along both radial and azimuthal axes. The azimuthal spin wave is characterized by a propagating spin-wave mode along the azimuthal axis, which can either be in the clockwise (CW) or counter-CW (CCW) sense<sup>23–25</sup>, with the frequency of the CW and CCW azimuthal modes shifted due to the coupling with the gyrotropic mode. Although vortex core switching via spin-wave mode excitation has been demonstrated on individual nanodots both optically<sup>24,28–32</sup> and via ferromagnetic resonance<sup>33,34</sup>, these modes have not been electrically characterized in fully integrated individual MTJs before, which is an essential step towards the realization of emerging ICT technologies.

## Results and discussion

**Dynamic behaviour in magnetic vortices.** In this study, we investigate the dynamics of magnetic vortices resonantly excited by the application of an rf current, with two excitation configurations: direct excitation of the rf current passing across the MTJ itself (Fig. 1a)<sup>35,36</sup> and indirect excitation via an integrated field line (Fig. 1b)<sup>37–39</sup>, with more device details presented in the ‘Methods’ section.

There are a variety of dynamic modes associated with the magnetic vortex, with the fundamental mode, known as the gyrotropic mode, characterized by an orbital motion of the vortex core around a fixed point as shown in Fig. 2a, where the magnetization along the z-axis is presented, as calculated with the Mumax<sup>340</sup> code. The polarity (negative) and chirality of the vortex are kept constant for all presented micromagnetic simulations. The gyrotropic mode is the only mode, which has successfully been excited to steady-state oscillations by the application of a dc current and has been shown to have the best spectral purity and output power of any STNO<sup>41</sup>. Traditionally, the gyrotropic mode in NiFe-based vortex MTJs operates in the 100–800 MHz band, which has the potential for neuromorphic applications<sup>42–46</sup> and local wireless sensor networks, but limits their impact for conventional wireless communications, such as WiFi and 5G frequency bands, which operate in GHz

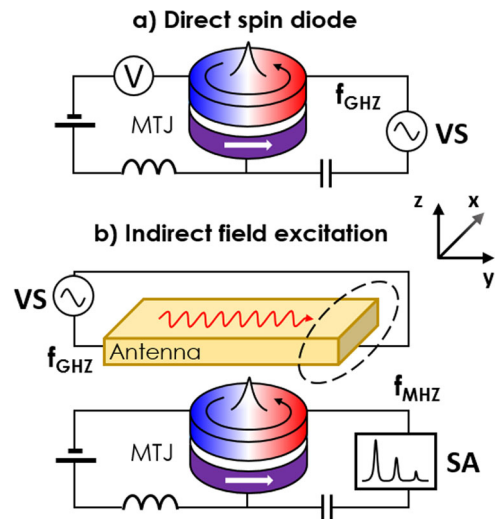


**Fig. 1 Device layout.** Schematic diagram of the high-frequency **a** direct spin diode and **b** indirect field excitation of the magnetic tunnel junction (MTJ), excited using a variable high-frequency source (VS) and measured either by a voltmeter (V) or a spectrum analyser (SA).

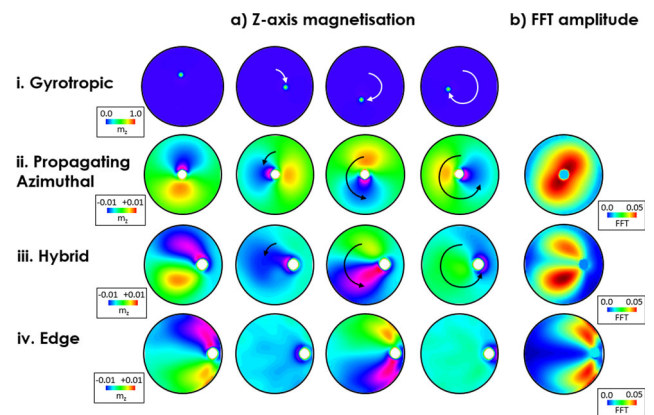


**Fig. 2 Dynamic modes in magnetic vortices.** **a** The different modes present in magnetic vortices depending upon the position of the vortex core. Images show the magnetization along the z-axis,  $m_z$ , calculated with micromagnetic simulations at four different times during the mode excitation and **b** the fast Fourier transform (FFT) amplitude of the respective modes.

frequency bands. Although recent work in ferrimagnets near the compensation point show higher frequencies<sup>47–49</sup>, additional work remains before this can be integrated into MTJ stacks.

In Fig. 2a, we expand upon the other high-frequency modes, which can be resonantly excited by direct spin-polarized current or an in-plane magnetic field (note that the radial spin-wave modes can only be directly excited by a perpendicular rf magnetic field<sup>50</sup>, which is not present in our system). As discussed previously, there is the azimuthal spin-wave mode, where a spin wave propagates in the body of the vortex around the vortex core. This behaviour can be clearly seen by constructing the FFT amplitude mode profile achieved with micromagnetic simulations (see Fig. 2b). This is achieved by exciting a specific mode via the application of a high-frequency in-plane magnetic field of 10  $\mu$ T and performing a Fourier transform of each cell as a function of time. The power of the high-frequency in-plane field has been chosen so as to be sufficiently low that no displacement of the vortex core is observed. For the propagating azimuthal mode, the FFT mode profile can be seen to be more or less continuous

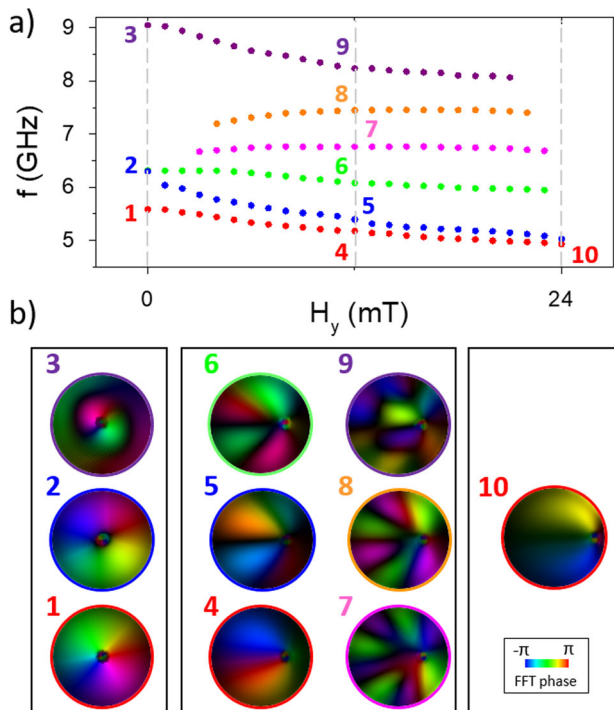


**Fig. 3 Higher-order mode field dependence.** **a** In-plane field,  $H_y$ , dependence of the various spin-wave mode frequencies,  $f$ , present in the nanopillar calculated with micromagnetic simulations and **b** bivariate fast Fourier transform (FFT) phase and amplitude images at selected frequencies and field.

around the vortex core. The region around the core has been removed for the sake of clarity.

If the vortex core becomes displaced from the centre of the nanopillar via the application of an in-plane magnetic field or during gyrotropic motion, the spatial profile of the mode becomes altered and there is an emergence of clear nodes and antinodes (see “Hybrid” in Fig. 2). The hybrid mode has both the node and anti-node modes characteristic of a standing wave, while retaining a sense of rotation. When the core is displaced further to the edge of the pillar, the mode profile more closely resembles that of a conventional edge mode<sup>51</sup>, with no clear sense of rotation (see “Edge” in Fig. 2), with the upper edge 180° out of phase with the lower edge.

The variation of the spin-wave modes as the vortex core is shifted is discussed in more detail in Fig. 3, where the simulated resonant frequency is plotted as a function of the in-plane magnetic field. Unlike Fig. 2, where only the FFT amplitude was plotted, in Fig. 3 we show the bivariate FFT amplitude and phase images to give a better understanding of the nature of the modes. At  $H_y = 0$  mT, three modes can be seen corresponding to the azimuthal propagating modes in both the CCW (labelled 1 at 5.5 GHz) and CW (labelled 2 at 6.3 GHz) directions, and at higher frequencies the hybridized azimuthal and radial spin-wave mode (labelled 3 at 9 GHz).

At an intermediate in-plane magnetic field, ( $H_y = 12$  mT), the available spin-wave modes have both azimuthal and standing wave characteristics, similar to the “hybrid” example discussed in Fig. 2. It is still possible to separate the modes with a CCW (labelled 4 at 5.3 GHz) and CW (labelled 5 at 5.6 GHz) senses of rotation; however, the frequencies of these two modes are starting to converge. At higher frequencies, there is an emergence of higher-order standing wave harmonics with four (labelled 6 at 6.1 GHz), six (labelled 7 at 6.8 GHz) and eight (labelled 8 at 7.5

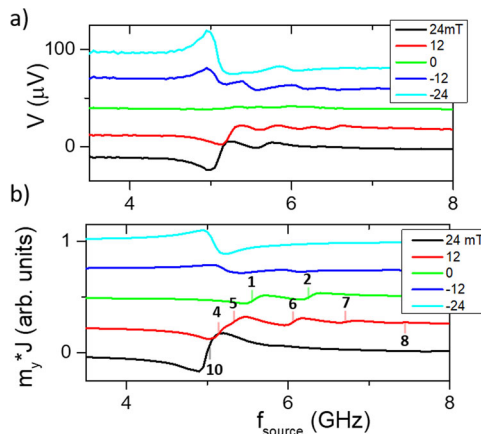


**Fig. 4 Rectification of higher-order modes.** **a** Experimental rectified voltage,  $V$ , and **b** the product of the magnetization along the  $y$ -axis,  $m_y$ , and the applied current density,  $J$ , as found with micromagnetic simulations as a function of excitation frequency,  $f_{\text{source}}$ , for different static in-plane magnetic fields. The  $y$ -axes are offset by 20  $\mu\text{V}$  for clarity.

GHz) antinodes visible. At even higher frequencies (labelled 9 at 8.3 GHz), there is a mode which has radial, azimuthal and standing wave characteristics. As the in-plane field is increased further (i.e.,  $H_y = 24$  mT), the two azimuthal spin-wave modes with opposite senses of rotation have almost fully converged such that there is mostly just one mode discernible, corresponding to the standing spin-wave edge mode (labelled 10 at 4.95 GHz).

**Rectification effect with higher-order modes.** In order to experimentally verify the behaviour of the higher-order modes in vortex-based MTJs, an rf current is passed across the MTJ (shown schematically in Fig. 1a), resulting in the so-called spin-torque diode effect<sup>52</sup>, where the applied rf current results in a rectified dc voltage if there is a corresponding resistance oscillation at the same frequency. In Fig. 4a, the measured rectified voltage as a function of the incoming frequency is shown for five different static in-plane magnetic fields applied along the  $y$ -axis, which is collinear to the pinning direction of the synthetic antiferromagnetic (SAF) layer. The dc voltages presented in Fig. 4a have been offset for clarity. The resultant rectified voltages are similar in magnitude to that observed for the gyrotropic mode, which has been extensively discussed in the literature<sup>35,36</sup>, and an example of which can be seen in the Supplementary Results (Fig. S11) for comparison.

In Fig. 4b, we present the time averaged product of the magnetization component along the  $y$ -axis and the applied rf current found using the micromagnetic simulations. There is good overall agreement between the micromagnetic simulations and the experimental data in terms of the lineshape of the frequency response with respect to various in-plane magnetic fields. For 0, 12 and 24 mT, the modes are labelled from 1 to 10 corresponding to the modes discussed in Fig. 3.

At zero in-plane applied magnetic field, the spin-torque diode rectified voltage and the corresponding simulations show a relatively small response, with the simulations showing two peaks corresponding to the two senses of rotation of the azimuthal modes. The mode labelled 3 was not observed, probably due to insufficient rf excitation of the mode located at such relatively high frequencies. As the static in-plane applied magnetic field is increased ( $H_y = 12$  mT), multiple peaks in the spin diode can be seen, which the simulations reproduce corresponding to the higher-order hybrid modes discussed previously. For a stronger static in-plane magnetic field ( $H_y = 24$  mT) the rectified spin-

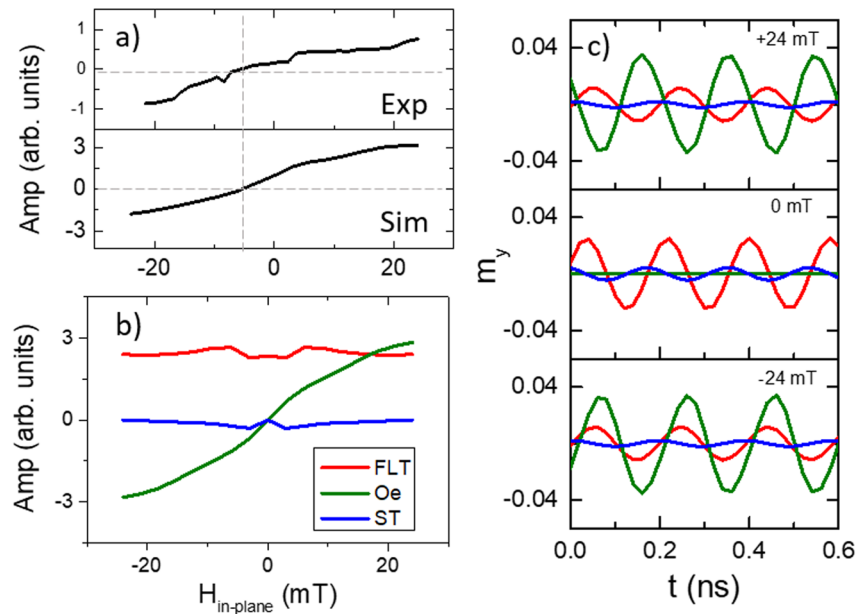


**Fig. 5 Resonant excitation mechanism.** **a** Lineshape amplitude, Amp, of the anti-Lorentz component of the lowest frequency peak as a function of static in-plane magnetic field for both experiment and micromagnetic simulations, **b** individual excitation mechanisms (i.e., Slonczewski (ST, blue), field-like (FLT, red) spin torques and radial Oersted field (Oe, green)) and **c** magnetization along the  $y$ -axis,  $m_y$ , as a function of time,  $t$ , for in-plane magnetic field,  $H_y = -24, 0$  and  $24$  mT.

diode voltage for the lowest-order peak becomes the largest, as the azimuthal modes converge and corresponds to the excitation of the standing wave edge mode.

In Fig. 4, the lineshape of the resonant response can be seen to change sign depending on the static in-plane field, which is discussed in more detail in Fig. 5, where the lowest frequency peak has been fit with an anti-Lorentzian lineshape. For a positive static in-plane magnetic field (i.e.,  $H_y = 24$  mT), the spin diode has a positive lineshape and for negative static in-plane magnetic fields (i.e.,  $H_y = -24$  mT) it has a negative lineshape. The sign of the anti-Lorentzian lineshape is plotted in Fig. 5a and has a quasi-linear field dependence, with a change of the sign of the lineshape at an in-plane field of  $H_y = -6$  mT. When analysing the micromagnetic simulations, there are three possible radio-frequency excitation mechanisms, the anti-damping Slonczewski (ST) and field-like (FLT) spin torques and the radial Oersted field (Oe).

To clarify the nature of these excitation mechanisms, in Fig. 5b the lineshape as a function of field for each excitation mechanism is presented. The ST spin torque results in a relatively small radiofrequency response, due to the anti-damping spin torque acting predominantly on the core rather than the body of the vortex<sup>36</sup>. The FLT acts to efficiently excite the higher-order modes relatively constantly for all values of static in-plane magnetic field. The radial OE field has a quasi-linear field dependence, as the excitation of the higher-order modes is related to the net magnetization, which is not collinear with the radial OE field (i.e., at  $H_y = 0$  mT, the radial OE field and the magnetization are collinear across the whole of the vortex and no excitation of the spin-wave modes occurs). The change in sign for the OE field can be seen in Fig. 5c, where the magnetization component as a function of time is presented for several static in-plane magnetic fields. The phase of the resultant magnetization displacement for the FLT torque is constant regardless of the in-plane field, but the phase changes by  $180^\circ$  for the radial OE field. An analogous effect can be seen for the different chiralities at similar static in-plane magnetic fields, where the lineshape also changes sign, as shown in the Supplementary Results (Fig. SI2). The lineshape is

independent of polarity (Figs. SI3 and SI4). The combination of the FLT torque and the radial OE field leads to the zero field offset and the quasi-linear field dependence.

To summarize the different excitation mechanisms, the radial OE field will not excite the ‘pure’ azimuthal spin-wave modes only found when the vortex is fully centred at  $H_y = 0$  mT; however, it is the dominant excitation mechanism of the edge modes. The FLT torque efficiently excites the ‘pure’ azimuthal, hybrid and edge spin-wave modes with similar efficiency, and the ST torque can be neglected for excitation of all spin-wave modes.

#### Coupling between the gyrotropic and higher-order modes.

Having identified the FLT torque as an efficient mechanism for the excitation of all the spin-wave modes present in the vortex-based STNO, in Fig. 6 we replace the direct excitation mechanism shown in Fig. 1a for the indirect excitation mechanism shown in Fig. 1b, where the rf current is passed through an adjacent integrated field line, producing an rf in-plane field collinear to that of the FLT torque. There are several advantages to the use of an integrated field line over direct current excitation, including easier impedance matching and greater breakdown current, allowing significantly higher excitation powers than are achievable with direct excitation, due to MTJ barrier degradation at higher rf powers.

Although we have previously demonstrated the excitation of the spin-wave modes directly, in Fig. 6 we show how the excitation of the spin-wave modes can indirectly affect the dynamic behaviour of the gyrotropic mode. There is a strong inter-mode coupling present in magnetic vortices, which has been previously shown optically to enable vortex core switching in individual nanodots<sup>29</sup>. This inter-mode coupling between the gyrotropic mode and the higher-order spin-wave modes is demonstrated in Fig. 6a, where the critical dc current necessary for the observation of a high-frequency voltage at the frequency of the gyrotropic mode (i.e., 190 MHz) is strongly modified by the excitation of the spin-wave modes.

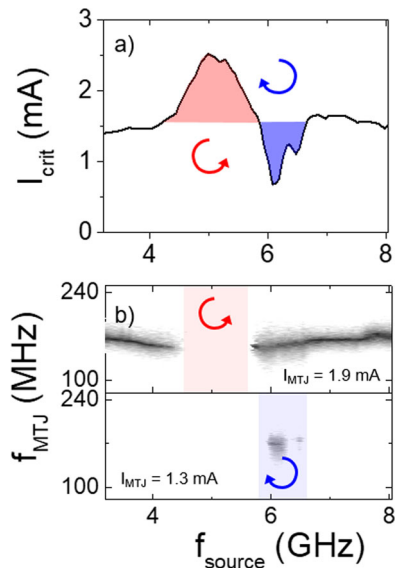


**Fig. 6 Gyrotropic critical current modified by higher-order mode excitation.**

**a** Critical current,  $I_{\text{crit}}$ , necessary to observe gyrotropic motion and **b** example spectra showing measured frequency,  $f_{\text{MTJ}}$ , vs. excitation frequency,  $f_{\text{source}}$ , for a super-critical ( $I_{\text{MTJ}} = 1.9$  mA) and a sub-critical ( $I_{\text{MTJ}} = 1.3$  mA) dc current of a magnetic tunnel junction, MTJ, with diameter  $d = 300$  nm. The circular arrows indicate the sense of propagation of the spin-wave mode.

The measurements were performed on a device with a diameter of  $d = 300$  nm and the excitation strength was  $P_{\text{antenna}}^{\text{rf}} = 4$  dBm. In the absence of a high-frequency magnetic field, the critical current is  $I_C = 1.45$  mA. When the spin-wave mode with an azimuthal sense of rotation contrary to the motion of the vortex core is excited (i.e., CCW = 5.1 GHz) the critical current necessary for gyrotropic motion of the core is significantly increased to  $I_C = 2.5$  mA. This can be clearly seen in the spectra presented in Fig. 6b, measured at a constant dc current of  $I_{\text{MTJ}} = 1.9$  mA, where the gyrotropic motion is suppressed when the mode at 5.1 GHz is excited. There is an opposite effect when the spin-wave mode with an azimuthal sense of rotation similar to the gyrotropic mode (i.e., CW = 6.1 GHz). In this case, the critical current is reduced and steady-state gyrotropic oscillations can be observed at a dc current as low as 0.6 mA. This effect is clearly demonstrated in the Fig. 6b, where a dc current of  $I_{\text{MTJ}} = 1.3$  mA is applied and the spectra is only measured around 6 GHz.

The effective damping of the gyrotropic vortex motion is therefore enhanced or reduced due to the coupling between the higher-order spin-wave modes and the gyrotropic mode depending upon the sense of propagation of the spin wave. This effect can be reproduced by the micromagnetic simulation, by a slight increase or decrease in the alpha damping term, shown in the Supplementary Results (Fig. SI5). As the vortex core is being excited to gyrotropic motion, it will be neither exactly at the centre or exactly at the edge of the pillar, and as such the mode being excited will be a hybridized azimuthal/edge mode, with standing wave nodes and antinodes, yet clearly it retains a sense of rotation as shown by the enhancement and reduction of the critical current for gyrotropic steady-state motion.

This modification in the critical current of the gyrotropic mode is further demonstrated in Fig. 7, where the power of the peak at the fundamental gyrotropic frequency ( $P_{\text{gyro}}$ ) is plotted as a function of the frequency ( $f_{\text{source}}$ ) and power ( $P_{\text{antenna}}^{\text{rf}}$ ) of the signal applied to the field line for a sub-critical ( $I_{\text{MTJ}} = 5$  mA) and super-critical ( $I_{\text{MTJ}} = 8$  mA) dc current on a  $d = 500$  nm device. In Fig. 7a, when the current is sub-critical (i.e.,  $I_{\text{MTJ}} = 5$  mA), the

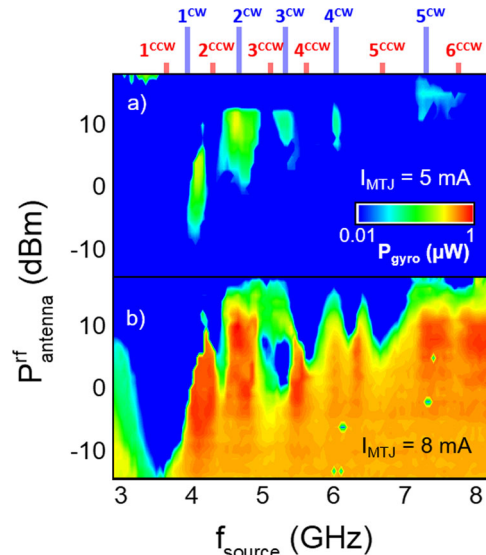


**Fig. 7 Power dependence of the mode coupling.** The measured power of the magnetic tunnel junction, MTJ, emission at the gyrotropic frequency,  $P_{\text{gyro}}$ , as a function of the rf excitation frequency,  $f_{\text{source}}$ , and power passed across the field line antenna,  $P_{\text{antenna}}^{\text{rf}}$ , for **a** a sub-critical ( $I_{\text{MTJ}} = 5$  mA) and **b** a super-critical dc current applied to the MTJ ( $I_{\text{MTJ}} = 8$  mA) for an MTJ of diameter,  $d = 500$  nm. The red and blue lines show the presence of modes with counter-clockwise (CCW) and clockwise (CW) sense of rotation of the spin-wave mode, respectively.

dc current is not enough to overcome the damping and generate steady gyrotropic motion, and there is no peak for low rf excitation powers. When a sufficiently strong rf signal is applied to the field line with the frequency of one of the spin-wave modes rotating with a CW sense of propagation, the effective critical current is reduced and the vortex core starts to enter a steady gyrotropic orbit, which results in a peak in the MHz range (i.e.,  $P_{\text{gyro}} > 0$ ). This effect can be seen to occur at several different excitation frequencies, which have been labelled from  $1^{\text{CW}}$  to  $5^{\text{CW}}$ . There is a general trend whereby the higher the frequency of the modes, the more rf power is required to produce a peak in the MHz range, which may relate to a reduction in the inter-mode coupling between the specific mode and the gyrotropic mode as the frequency difference increases.

When a super-critical current is applied (i.e.,  $I_{\text{MTJ}} = 8$  mA), the opposite behaviour is observed as shown in Fig. 7b, where at certain GHz excitation frequencies (labelled  $1^{\text{CCW}}$  to  $6^{\text{CCW}}$ ) the MHz peak completely disappears (i.e.,  $P_{\text{gyro}} = 0$ ) when the spin-wave modes corresponding to a CCW sense of propagation are sufficiently excited. The frequencies of the corresponding CCW modes are slightly lower than the corresponding CW modes, which is consistent with the behaviour expected for the hybrid azimuthal mode, discussed in Fig. 6.

## Conclusion

In conclusion, magnetic vortex-based spin-torque oscillators are a rich dynamic system with many different accessible high-frequency modes, the nature of which is highly dependent on the location of the vortex core, shifting from a ‘pure’ azimuthal mode to a standing edge mode. These modes are experimentally investigated directly via the spin-torque diode effect, where it is found that the FLT torque is the dominant excitation mechanism when the vortex core is located at the centre of the pillar, but with the OE field becoming increasingly dominant as the core approaches the edge of the nanopillar. In addition, the inter-mode coupling between the higher-order modes and the fundamental gyrotropic mode is

explored, where the sense of rotation of the higher-order mode has been shown to control the effective damping of the gyrotropic mode for six different spin-wave modes. The ability of these devices to act as rectifiers or to modify the gyrotropic current demonstrates the potential of super high-frequency applications utilizing vortex-based MTJ devices, which have long been considered limited to the sub-GHz frequency range.

## Methods

**Device details.** The devices under investigation are MTJs with a CoFe(2.0)/Ru(0.7)/CoFeB(2.6 nm) SAF acting as the pinned layer and a CoFeB(2.0)/Ta(0.2)/NiFe(7.0 nm) composite layer as the free layer separated by a thin MgO(1.0 nm) layer<sup>37,39</sup>. For diameters greater than  $d > 300$  nm, the magnetic ground state of the free layer is the magnetic vortex, where the in-plane component of the magnetization forms a closed loop, whereas the magnetization of the central region of the vortex, i.e., the vortex core, tilts perpendicular to the plane. Nanopillars from 300 to 1000 nm in diameter were investigated and similar behaviour was observed.

**Excitation mechanism.** The magnetic vortex is resonantly excited by an applied rf current, with two excitation configurations: direct excitation of the rf current passing across the MTJ itself (Fig. 1a)<sup>35,36</sup> and indirect excitation via an integrated field line (Fig. 1b)<sup>37–39</sup>. For the direct excitation configuration, there are three potential excitation mechanisms, the OE field produced by the current, and the anti-damping and the FLT spin-torque terms<sup>7</sup>. For the integrated field line, the coupling between the current and the magnetic vortex occurs as the current induces an in-plane magnetic field, which is felt by the vortex, located ~300 nm below the field line. The field produced by the indirect field line excitation configuration is collinear to the FLT spin-torque produced by the direct current configuration, i.e., collinear to the pinning axis of the SAF<sup>37</sup>.

## Data availability

The data that support the findings of this study are available from the corresponding author upon request.

Received: 30 October 2020; Accepted: 30 March 2021;

Published online: 25 May 2021

## References

- Kiselev, S. I. et al. Microwave oscillations of a nanomagnet driven by a spin-polarized current. *Nature* **425**, 380 (2003).
- Pribyl, V. S. et al. Magnetic vortex oscillator driven by d.c. spin-polarized current. *Nat. Phys.* **3**, 498 (2007).
- Houssameddine, D. et al. Spin-torque oscillator using a perpendicular polarizer and a planar free layer. *Nat. Mater.* **6**, 447 (2007).
- Quinsat, M. et al. Amplitude and phase noise of magnetic tunnel junction oscillators. *Appl. Phys. Lett.* **97**, 182507 (2010).
- Dussaux, A. et al. Large microwave generation from current-driven magnetic vortex oscillators in magnetic tunnel junctions. *Nat. Commun.* **1**, 1 (2010).
- Quinsat, M. et al. Modulation bandwidth of spin torque oscillators under current modulation. *Appl. Phys. Lett.* **105**, 152401 (2014).
- Dussaux, A. et al. Large amplitude spin torque vortex oscillations at zero external field using a perpendicular spin polarizer. *Appl. Phys. Lett.* **105**, 022404 (2014).
- Costa, J. D. et al. High power and low critical current density spin transfer torque nano-oscillators using MgO barriers with intermediate thickness. *Sci. Rep.* **7**, 7237 (2017).
- Tarequzzaman, M. et al. Spin torque nano-oscillator driven by combined spin injection from tunneling and spin Hall current. *Commun. Phys.* **2**, 20 (2019).
- Chumak, A. V., Vasyuchka, V. I., Serga, A. A. & Hillebrands, B. Magnon spintronics. *Nat. Phys.* **11**, 453 (2015).
- Rippard, W., Pufall, M., Kaka, S., Russek, S. & Silva, T. Direct-current induced dynamics in Co 90 Fe 10/Ni 80 Fe 20 point contacts. *Phys. Rev. Lett.* **92**, 027201 (2004).
- Demidov, V. E., Urazhdin, S., Anane, A., Cros, V. & Demokritov, S. O. Spin-orbit-torque magnonics. *J. Appl. Phys.* **127**, 170901 (2020).
- Demidov, V. E. et al. Excitation of coherent propagating spin waves by pure spin currents. *Nat. Commun.* **7**, 10446 (2016).
- Kaka, S. et al. Mutual phase-locking of microwave spin torque nano-oscillators. *Nature* **437**, 389 (2005).
- Houssang, A. et al. Spin-wave-beam driven synchronization of nanocontact spin-torque oscillators. *Nat. Nanotechnol.* **11**, 280 (2016).
- Behncke, C. et al. Spin-wave interference in magnetic vortex stacks. *Commun. Phys.* **1**, 1 (2018).
- Wintz, S. et al. Magnetic vortex cores as tunable spin-wave emitters. *Nat. Nanotechnol.* **11**, 948 (2016).
- Hertel, R. & Schneider, C. M. Exchange explosions: magnetization dynamics during vortex-antivortex annihilation. *Phys. Rev. Lett.* **97**, 177202 (2006).
- Choi, S., Lee, K. S., Guslienko, K. Y. & Kim, S. K. Strong radiation of spin waves by core reversal of a magnetic vortex and their wave behaviors in magnetic nanowire waveguides. *Phys. Rev. Lett.* **98**, 087205 (2007).
- Novosad, V. et al. Spin excitations of magnetic vortices in ferromagnetic nanodots. *Phys. Rev. B Condens. Matter Mater. Phys.* **66**, 524071 (2002).
- Guslienko, K. Y., Scholz, W., Chantrell, R. W. & Novosad, V. Vortex-state oscillations in soft magnetic cylindrical dots. *Phys. Rev. B Condens. Matter Mater. Phys.* **71**, 144407 (2005).
- Taurel, B. et al. Complete mapping of the spin-wave spectrum in a vortex-state nanodisk. *Phys. Rev. B* **93**, 184427 (2016).
- Guslienko, K. Y., Slavin, A. N., Tiberkevich, V. & Kim, S. K. Dynamic origin of azimuthal modes splitting in vortex-state magnetic dots. *Phys. Rev. Lett.* **101**, 1 (2008).
- Hoffmann, F. et al. Mode degeneracy due to vortex core removal in magnetic disks. *Phys. Rev. B* **76**, 014416 (2007).
- Park, J. P. & Crowell, P. A. Interactions of spin waves with a magnetic vortex. *Phys. Rev. Lett.* **95**, 1 (2005).
- Yoo, M.-W., Lee, J. & Kim, S.-K. Radial-spin-wave-mode-assisted vortex-core magnetization reversals. *Appl. Phys. Lett.* **100**, 172413 (2012).
- Giovannini, L. et al. Spin excitations of nanometric cylindrical dots in vortex and saturated magnetic states. *Phys. Rev. B - Condens. Matter Mater. Phys.* **70**, 1 (2004).
- Park, J. P., Eames, P., Engebretson, D. M., Berezovsky, J. & Crowell, P. A. Imaging of spin dynamics in closure domain and vortex structures. *Phys. Rev. B* **67**, 020403 (2003).
- Kammerer, M. et al. Magnetic vortex core reversal by excitation of spin waves. *Nat. Commun.* **2**, 279 (2011).
- Bauer, H. G., Sproll, M., Back, C. H. & Woltersdorf, G. Vortex core reversal due to spin wave interference. *Phys. Rev. Lett.* **112**, 1 (2014).
- Buess, M. et al. Excitations with negative dispersion in a spin vortex. *Phys. Rev. B Condens. Matter Mater. Phys.* **71**, 1 (2005).
- Vogt, K. et al. Optical detection of vortex spin-wave eigenmodes in microstructured ferromagnetic disks. *Phys. Rev. B Condens. Matter Mater. Phys.* **84**, 174401 (2011).
- Dutra, R. et al. Spin wave dynamics in elliptical dots. *Phys. Rev. B* **99**, 014413 (2019).
- Aliev, F. G. et al. Spin waves in circular soft magnetic dots at the crossover between vortex and single domain state. *Phys. Rev. B Condens. Matter Mater. Phys.* **79**, 174433 (2009).
- Jenkins, A. S. et al. Controlling the chirality and polarity of vortices in magnetic tunnel junctions. *Appl. Phys. Lett.* **105**, 172403 (2014).
- Jenkins, A. S. et al. Spin-torque resonant expulsion of the vortex core for an efficient radiofrequency detection scheme. *Nat. Nanotechnol.* **11**, 360 (2016).
- Jenkins, A. S. et al. Wideband high-resolution frequency-to-resistance converter based on nonhomogeneous magnetic-state transitions. *Phys. Rev. Appl.* **13**, 014046 (2020).
- Jenkins, A. S., Alvarez, L. S. E., Freitas, P. P. & Ferreira, R. Nanoscale true random bit generator based on magnetic state transitions in magnetic tunnel junctions. *Sci. Rep.* **9**, 15661 (2019).
- Jenkins, A. S., Alvarez, L. S. E., Freitas, P. P. & Ferreira, R. Digital and analogue modulation and demodulation scheme using vortex-based spin torque nano-oscillators. *Sci. Rep.* **10**, 1 (2020).
- Vansteenkiste, A. et al. Waeyenberge, The design and verification of MuMax3. *AIP Adv.* **4**, 107133 (2014).
- Tsunegi, S., Yakushiji, K., Fukushima, A., Yuasa, S. & Kubota, H. Microwave emission power exceeding 10  $\mu$ W in spin torque vortex oscillator. *Appl. Phys. Lett.* **109**, 252402 (2017).
- Torrejon, J. et al. Neuromorphic computing with nanoscale spintronic oscillators. *Nature* **547**, 428 (2017).
- Locatelli, N., Cros, V. & Grollier, J. Spin-torque building blocks. *Nat. Mater.* **13**, 11 (2014).
- Romera, M. et al. Vowel recognition with four coupled spin-torque nano-oscillators. *Nature* **563**, 230–234 (2018).
- Lebrun, R. et al. Mutual synchronization of spin torque nano-oscillators through a long-range and tunable electrical coupling scheme. *Nat. Commun.* **8**, 15825 (2017).
- Farkhani, H. et al. LAO-NCS: laser assisted spin torque nano oscillator-based neuromorphic computing system. *Front. Neurosci.* **13**, 1429 (2020).
- Kim, S. K. & Tserkovnyak, Y. Fast vortex oscillations in a ferrimagnetic disk near the angular momentum compensation point. *Appl. Phys. Lett.* **111**, 032401 (2017).
- Ivanov, B. A. Ultrafast spin dynamics and spintronics for ferrimagnets close to the spin compensation point (Review). *Low Temp. Phys.* **45**, 935–963 (2019).

49. Carvajal, D. A., Riveros, A. & Escrig, J. Orbit-like trajectory of the vortex core in ferrimagnetic dots close to the compensation point. *Results Phys.* **19**, 103598 (2020).
50. Zhu, X., Liu, Z., Metlushko, V., Grütter, P. & Freeman, M. R. Broadband spin dynamics of the magnetic vortex state: effect of the pulsed field direction. *Phys. Rev. B* **71**, 180408(R) (2005).
51. Keatley, P. S. et al. Large amplitude magnetization dynamics and the suppression of edge modes in a single nanomagnet. *Appl. Phys. Lett.* **98**, 082506 (2011).
52. Tulapurkar, A. A. et al. Spin-torque diode effect in magnetic tunnel junctions. *Nature* **438**, 339 (2005).

### Acknowledgements

A.S.J. and R.F. gratefully acknowledge the NORTE-01-0145-FEDER-000019 project, and L.S.E.A. received funding from MSCA-COFUND-2015-FP-713640 and A.S.J. received funding from NOVAMAG (SAICT/030085/2017). V.C. and P.B. acknowledge the French ANR project "SPINNET" ANR-18-CE24-0012 for the support to this work.

### Author contributions

Devices were fabricated by L.S.E.A. and R.F., and data analysis was performed by A.S.J., S.M., P.B., V.C., P.P.F., and R.F. Simulations were performed by A.S.J. The manuscript was prepared by A.S.J. with feedback from the other authors.

### Competing interests

The authors declare no competing interests.

### Additional information

**Supplementary information** The online version contains supplementary material available at <https://doi.org/10.1038/s42005-021-00614-3>.

**Correspondence** and requests for materials should be addressed to A.S.J.

**Reprints and permission information** is available at <http://www.nature.com/reprints>

**Publisher's note** Springer Nature remains neutral with regard to jurisdictional claims in published maps and institutional affiliations.



**Open Access** This article is licensed under a Creative Commons Attribution 4.0 International License, which permits use, sharing, adaptation, distribution and reproduction in any medium or format, as long as you give appropriate credit to the original author(s) and the source, provide a link to the Creative Commons license, and indicate if changes were made. The images or other third party material in this article are included in the article's Creative Commons license, unless indicated otherwise in a credit line to the material. If material is not included in the article's Creative Commons license and your intended use is not permitted by statutory regulation or exceeds the permitted use, you will need to obtain permission directly from the copyright holder. To view a copy of this license, visit <http://creativecommons.org/licenses/by/4.0/>.

© The Author(s) 2021